



1 **Palaeoclimate significance of speleothems in crystalline rocks:**
2 **a test case from the Lateglacial and Early Holocene**
3 **(Vinschgau, northern Italy)**

4 Gabriella Koltai^{1*}, Hai Cheng², Christoph Spötl¹

5 ¹ Institut für Geologie, Leopold-Franzens-Universität Innsbruck, Innrain 52, 6020 Innsbruck, Austria

6 ² Xi'an Jiaotong University, School of Human Settlement and Civil Engineering, Shaanxi, China

7 *Correspondence to:* gabriella.koltai@uibk.ac.at

8

9 **Abstract:** Coeval flowstones formed in fractured gneiss and schist were studied to test the palaeoclimate
10 significance of this new type of speleothem archive on a decadal to millennial timescale. The samples encompass
11 a few hundred to a few thousand years of the Lateglacial and the Early Holocene. The speleothem fabric is
12 primarily comprised of columnar fascicular optic calcite and acicular aragonite, both being indicative of elevated
13 Mg/Ca ratios in the groundwater. Stable isotopes suggest that aragonite is more prone to kinetic isotope
14 fractionation driven by evaporation and prior calcite/aragonite precipitation than calcite. Changes in mineralogy
15 are also attributed to these two aquifer-internal processes rather than to palaeoclimate. Flowstones formed in the
16 same fracture show similar $\delta^{18}\text{O}$ changes on centennial scales, which broadly correspond to regional lacustrine
17 $\delta^{18}\text{O}$ records (e.g. Mondsee), suggesting that such speleothems may provide an opportunity to investigate past
18 climate conditions in non-karstic areas. The shortness of overlapping periods in flowstone growth and the
19 complexity of in-aquifer processes, however, render the establishment of a robust stacked $\delta^{18}\text{O}$ record
20 challenging.

21 **1 Introduction**

22 Speleothems from karst caves have contributed important information on past climate change from orbital to
23 seasonal time scales worldwide by yielding high-resolution, multi-proxy data (e.g. Johnson et al., 2006; Boch et
24 al., 2011; Fohlmeister et al., 2012; Wang et al., 2014; Webb et al., 2014; Luetscher et al., 2015; Cheng et al.,
25 2016). While the importance of these speleothems as palaeoclimate archives is firmly established, very little is
26 known about the palaeoclimate potential of such deposits from non-carbonate settings. Since only ~ 20% of the
27 ice-free continental area of the Earth consists of carbonate rocks prone to karstification (Ford and Williams,
28 2007) speleothems from non-karstic settings may provide relevant palaeoclimate archives for semi-arid (Koltai
29 et al., 2017) to subglacial environments (Frisia et al., 2017).

30 In comparison to other palaeoclimate archives, a key advantage of speleothems is that they can be dated with
31 high precision by U-Th techniques up to about half a million years (e.g. Richards and Dorale, 2003; Scholz and
32 Hoffmann, 2008; Cheng et al., 2013). Since silicate rocks usually contain much more uranium than limestones or
33 dolostones, the ²³⁸U content of speleothems forming in cavities and fractures of crystalline rocks is commonly
34 orders of magnitude higher (Wedepohl, 1995), and therefore require very little sample amount to yield high
35 resolution chronologies (Spötl et al., 2002; Koltai et al., 2017).

36 Here, we present a well-dated, multi-proxy record of eight fast growing flowstones from a non-karstic setting in
37 the Vinschgau, located south of the main crest of the Alps. Unlike speleothems formed in karst caves, these



1 calcite and aragonite flowstones were deposited in near-surface fractures created by gravitational mass
2 movements (Ostermann et al., submitted). The aim of our study is to test the reliability of climate proxies
3 preserved in this hitherto largely neglected type of speleothem archive.

4 To assess the fidelity of our proxy data as a record of past climate changes we selected the Lateglacial to Early
5 Holocene time interval. We take advantage of the fact that the Younger Dryas (YD) is among the most
6 extensively studied periods in the late Quaternary due to the widespread availability of high-resolution
7 palaeoclimate records such as ice cores, marine and lake sediment cores (Dansgaard et al., 1989; Alley et al.,
8 2000; Brauer et al., 2008; Broecker et al., 2010; Schlolaut et al., 2017).

9 In the Alps, most high-resolution terrestrial climate information about rapid changes of the Lateglacial and
10 Termination I has been derived from studies of lake sediments (e.g., von Grafenstein et al., 1999, 2013; Magny
11 et al., 2001; Ilyashuk et al., 2009; Lauterbach et al., 2011; Heiri et al., 2014), complemented by palaeoglacier
12 (e.g., Kerschner et al., 2000; Ivy-Ochs et al., 2008; Kerschner and Ivy-Ochs, 2008) and speleothem records
13 (Wurth et al., 2004; Luetscher et al., in prep.). By comparing the Vinschgau speleothem data to additional
14 Lateglacial and the Early Holocene records, we aim to explore the extent to which Vinschgau speleothems
15 record the well-documented succession of rapid climate change during these time periods, or are subject to site-
16 specific processes alone. To this end, a multi-proxy approach using petrographic and geochemical analyses is
17 applied.

18 **2 Site description and samples**

19 **2.1 Study site**

20 The Vinschgau is a W-E trending inner-alpine valley shielded by high mountain chains in the north, west and
21 south. Although it is one of the driest valleys of the Eastern Alps today (Fliri, 1975; ZAMG, 2015), local climate
22 archives such as large debris-flow fans (which are largely inactive today) point to periods of distinctly more
23 humid climate during the Lateglacial and Holocene in this valley. This is further corroborated by the presence of
24 deep and steep gullies dissecting the south-facing flank of the valley that formed after the deglaciation of the
25 valley.

26 The study area is comprised of paragneiss, orthogneiss and schists that are heavily fractured as a result of deep-
27 seated gravitational mass movements along the Sonnenberg. These fractures provide pathways for groundwater
28 flow. Due to pronounced water-rock interaction dominated by pyrite oxidation and the presence of large internal
29 mineral surfaces created by mass movements, these waters are highly mineralized. Speleothems and tufa form on
30 the south-facing Sonnenberg slope where groundwater reaches supersaturation in the shallow subsurface due to
31 evaporation and concomitant CO₂ degassing (Spötl et al., 2002; Koltai et al., 2017).

32 **2.2 Speleothem samples**

33 Eight vein-filling flowstones were obtained from three different fractures (Fig. 1). It must be emphasized that the
34 samples were not collected in-situ from the fractures, thus their exact position within these fractures is unknown.
35 LAS 1, LAS 2 and LAS 21 were collected at Törgltal (TR), while LAS 6, LAS 34 and LAS 72 are from
36 Stollenquelle (SQ). These two sites are less than 1 km apart. The third fracture (Kortsch-KO) is situated
37 approximately 5 km east of SQ. Two samples (LAS 10 and LAS 19) were collected there.



1 Aragonite is present near the top of samples LAS 2, LAS 6 and LAS 21. Thus, the uppermost 12, 15 and 6 mm
2 of LAS 2, LAS 6 and LAS 21, respectively, were not included in this study. As LAS 10 grew between $9.26 \pm$
3 0.10 ka and 10.22 ± 0.06 ka according to the depth-age model, the present study focuses only on the lower 21.4
4 mm of this flowstone.

5 **3 Methods**

6 **3.1 Petrography**

7 Thin sections were analysed under transmitted-light and blue-light epifluorescence microscopy in order to
8 identify characteristic fabrics and areas of replacement of aragonite by calcite. Furthermore, small aliquots of
9 carbonate powder were obtained from LAS 2, LAS 6 and LAS 34 using a hand-held dental drill in order to
10 determine the mineralogical composition by X-ray diffractometry (XRD).

11 **3.2 Stable isotopes**

12 Samples for stable oxygen and carbon isotope analyses were micromilled at different resolutions. LAS 2 was
13 sampled at 0.1 mm intervals, LAS 1, LAS 6, LAS 34 and LAS 72 were micromilled at 0.15 mm increments. In
14 order to reach a multi-annual resolution (3 years) LAS 6 was also analysed by using three 2.5 mm-long parallel
15 tracks milled with a 0.8 mm offset perpendicular to the lamination. LAS 10 and LAS 19 were analysed at 0.2
16 mm, while LAS 21 was analysed at 0.25 mm resolution. Stable isotope measurements were performed using a
17 Thermo Fisher Scientific DELTA^{plus}XL mass spectrometer. Isotope values are reported against the VPDB scale
18 and the long-term analytical precision (1σ) of the $\delta^{18}\text{O}$ and $\delta^{13}\text{C}$ measurements is 0.08 and 0.06‰, respectively
19 (Spötl, 2011).

20 **3.3 U-Th dating**

21 A total of 77 powder samples were prepared for radiometric dating. If present, primary aragonite was preferred
22 over calcite, since aragonite-to-calcite transformation may alter the geochemical composition (e.g. Lachniet et
23 al., 2012; Domínguez-Villar et al., 2016). U-Th dates were divided amongst samples as follows: eleven dates
24 measured from LAS 2 and LAS 6, ten from LAS 1, eight from LAS 10 and LAS 21, fourteen from LAS 19, nine
25 from LAS 72, and six from LAS 34. Aliquots were obtained for U-Th dating from distinct growth layers using a
26 handheld drill. The weight of individual subsamples ranged between 1.0 and 9.0 mg.

27 The samples were analysed at the Xi'an Jiaotong University (China) following standard chemistry procedures of
28 Edwards et al. (1987) to separate uranium and thorium. U and Th isotopes were analysed individually by using a
29 multicollector inductively coupled plasma mass spectrometer (Thermo Fischer Neptune Plus) as described by
30 Shen et al. (2012) and Cheng et al. (2013). Final ^{230}Th ages are given with their 2σ uncertainties as years before
31 1950 AD (BP). Corrected and uncorrected results are given in Suppl. Table 1. Corrected ages assume an initial
32 $^{230}\text{Th}/^{232}\text{Th}$ ratio of $4.4 \pm 2.2 \times 10^{-6}$ of bulk Earth (Wedepohl, 1995). Separate age models for all samples were
33 built using the StalAge algorithm (Scholz and Hoffman, 2011).



1 **4 Results**

2 **4.1 Petrography**

3 The crystal fabric of LAS 6, LAS 10 and LAS 19 is dominated by columnar fascicular optic calcite (Cfo; Frisia,
4 2015), showing undulose extinction due to the systematic change in the orientation of the c-axes (Kendall, 1985;
5 Richter et al., 2011; Frisia, 2015). Detrital-rich layers are locally present in LAS 10 and LAS 19. Their average
6 thickness varies from 25 to 50 μm in LAS 10 and between 50 and 75 μm in LAS 19, however, in the latter
7 sample detrital-rich layers up to 0.25 mm wide are also present.

8 LAS 72 is comprised of white acicular aragonite, while translucent calcite is also present in LAS 1, 2, 21 and 34.
9 In LAS 2 both primary and secondary calcite were identified by thin section analyses (Fig. 2a-b). Secondary
10 calcite is mostly present at the aragonite-calcite transitions. XRD results indicate 100% calcite in the calcite
11 layers of LAS 2 and 34. In other parts of LAS 2 and also in LAS 21 aragonite islands that are locally present in
12 the calcite fabric and show no sign of dissolution suggesting co-precipitation of aragonite and calcite (Fig. 2c).
13 LAS 6, 10, 19 and 21 do not show any sign of diagenetic alteration.

14 Thin-section analyses of LAS 34 revealed the presence of mosaic calcite (Fig. 2d), a fabric indicative of
15 recrystallisation (e.g. Frisia, 2015). As recrystallization may have modified the geochemical composition of the
16 calcite, only the aragonite fabric is discussed further in this study.

17 From the 60 until 110 mm dft LAS 6 exhibits annual calcite lamina couplets which can be observed
18 macroscopically as successive white and translucent laminae. The white laminae are rich in opaque particles,
19 whose organic origin is confirmed by their strong epifluorescence (Koltai et al., 2017). Similarly, the inclusion-
20 rich layers in the fascicular optic calcite of LAS 10 and LAS 19 show excitation under epifluorescence.
21 Furthermore, weakly fluorescent laminae are present in LAS 72, while both calcite and aragonite layers in LAS 2
22 and LAS 21 appear dull.

23 **4.2 Stable isotope composition**

24 The summarized results of the stable isotope analyses are presented in Table 1. High-resolution stable isotope
25 profiles of the flowstones collected near TR show very similar values for $\delta^{18}\text{O}$, while carbon isotope values are
26 more diverse. Even though $\delta^{13}\text{C}$ minima are identical within the 1σ analytical error in these samples, the highest
27 carbon isotope values range from 2.4 to 7.3 ‰ (Table 1).

28 As Table 1 shows, the SQ samples are characterised by different values regarding both $\delta^{18}\text{O}$ and $\delta^{13}\text{C}$. The two
29 flowstones dominated by aragonite (LAS 34 and LAS 72) exhibit more enriched isotope values, while the calcite
30 samples from KO are characterised by the most depleted $\delta^{13}\text{C}$ values.

31 The majority of the flowstones do not exhibit a correlation between $\delta^{13}\text{C}$ and $\delta^{18}\text{O}$ values, with the exception of
32 three samples (LAS 2, LAS 34 and LAS 72) which show a significant correlation between the two isotopes (Fig.
33 3). The crystal fabric of these samples is dominated by acicular aragonite. In LAS 2 the covariance of $\delta^{13}\text{C}$ and
34 $\delta^{18}\text{O}$ is characterised by almost identical slopes of the regression lines for both aragonite and calcite (Fig. 3). On
35 the contrary, LAS 1 does not show any covariance for calcite ($R^2=0.33$) and aragonite ($R^2=0.13$). The number of
36 stable isotopes analyses ($n=7$) in the aragonite of LAS 21 was too small to investigate the relationship of $\delta^{13}\text{C}$
37 and $\delta^{18}\text{O}$ variability.

38 Carbon isotope values mostly follow the first-order changes of oxygen isotopes in all samples except LAS 1.
39 However, the relationship between the two isotopes may vary within a given sample. In LAS 6 and LAS 21 this



1 relationship breaks down in the topmost 13 and 7 mm distance from top (dft), respectively, while in LAS 19
2 rising $\delta^{18}\text{O}$ values correspond to decreasing $\delta^{13}\text{C}$ levels from 66 to 54 mm (dft).
3 Major changes in $\delta^{18}\text{O}$ values are observed in LAS 2 and LAS 19. The former sample exhibits generally high
4 oxygen isotope values in the aragonite growth phase from the bottom until 50 mm (dft), interrupted by periods of
5 lower $\delta^{18}\text{O}$ values. A 0.8 ‰ decrease is seen between 74 and 72 mm (dft) coinciding with the presence of a
6 calcite layer. A gradual shift of 2.2 ‰ towards more negative values is observed from 52 to 47 mm (dft) and is
7 independent of the fabric, while a 1.6 ‰ rise in $\delta^{18}\text{O}$ characterises the calcite from 17 to 14 mm (dft). In LAS 19
8 a significant 3.2 ‰ shift towards more positive $\delta^{18}\text{O}$ values occurs from 66 to 54 mm (dft), followed by a
9 decrease in carbon isotope values. Moreover, in all samples $\delta^{18}\text{O}$ values show high-frequency changes of
10 different amplitude (0.5 to 1.5 ‰) while no major trend is observed.

11 4.3 Chronology

12 The Vinschgau samples show exceptionally high ^{238}U concentrations, ranging from ca. 1.5 to 1200 ppm (Table
13 1) and are among the most U-rich speleothems ever reported (Spötl et al., 2002; Kelly et al., 2003). $\delta^{234}\text{U}$ ranges
14 from 7 to 100 ‰. The ^{232}Th content is highly variable and fluctuates between 61 ppt and 178 ppb (Suppl. Table
15 1). Except for three subsamples of LAS 19 all samples show high $^{230}\text{Th}/^{232}\text{Th}$ activity ratios and thus, excess
16 ^{230}Th has no significant influence on the final ages.

17 Of the 77 total dates measured, 74 are in stratigraphic order within their 2σ uncertainties. The three dated offsets
18 (from samples L6-54, L6-79 and L1-38.5) are 5, 2 and 60 years beyond stratigraphic order, respectively (Suppl.
19 Table 1). As these differences represent less than 0.5, 0.25 and ~2‰ age deviation for L6-54, L6-79 and LAS 34,
20 respectively, we do not consider these ages as outliers and include them in the age models (Suppl. Figs. 1-2).

21 LAS 1 formed between 12.99 ± 0.05 and 12.01 ± 0.03 ka, while LAS 2 grew uninterruptedly between $14.18 \pm$
22 0.03 and 12.12 ± 0.03 ka. The last sample from the TR site, LAS 21 initiated deposition at 12.28 ± 0.03 and grew
23 continuously until 11.68 ± 0.02 ka BP (Suppl. Figs. 1-2).

24 LAS 6 from the SQ site formed between 12.06 ± 0.04 and 11.68 ± 0.03 ka. Similarly to LAS 2, growth of LAS
25 34 commenced 14.18 ± 0.03 ka and ended 12.54 ± 0.03 ka, showing no major growth interruptions, while LAS
26 72 provides a record between 11.64 ± 0.04 and 10.03 ± 0.03 ka (Suppl. Figs. 1-2).

27 The U-Th dates of the studied section of LAS 10 range from 9.94 ± 0.03 to 10.21 ± 0.06 ka, while LAS 19
28 started to form in the YD at 11.98 ± 0.05 ka and stopped growing in the Early Holocene at 10.78 ± 0.04 ka
29 (Suppl. Fig. 5).

30 5 Discussion

31 5.1 Stable isotope systematics

32 5.1.1 $\delta^{18}\text{O}$

33 In karstic settings, speleothem $\delta^{18}\text{O}$ values depend on the $\delta^{18}\text{O}$ composition of drip water and the cave air
34 temperature, the latter influencing water-carbonate fractionation factors for both calcite and aragonite (e.g.
35 McDermott, 2004; Lachniet, 2015). Modern spring monitoring in the Vinschgau suggests that the speleothem-
36 forming waters are part of a larger groundwater system recharging at an elevation ranging from about 1200 to
37 2100 m a.s.l. Minimal variation in stable isotope composition and low tritium content point to long mean
38 residence times of up to several decades (Spötl et al., 2002).



1 5% of the studied flowstone samples (e.g. LAS 6) exhibit annual petrographic and geochemical lamination.
2 Stable isotope analyses and heat-transfer modelling indicate that their $\delta^{18}\text{O}$ oscillations are dominated by surface
3 temperature changes transmitted to the subsurface via heat conduction (Koltai et al., 2017). As the well-
4 developed petrographic lamination is due to traces of varying amounts of humic and fulvic acids, the lack of
5 such regular laminae can be used as an indirect proxy for the depth of a given fracture. Except for LAS 6, none
6 of the flowstones exhibit regular lamination. Thus we assume that non-laminated flowstones formed at greater
7 depths and the temperature in these subsurface fractures most likely reflects the outside mean annual air
8 temperature. Spötl et al. (2002) reported that none of the nearby perennial spring showed intra-annual
9 temperature variability, supporting this assumption. The water temperature of such a spring at the SQ site was
10 constant during the two-year-long monitoring period. Water dripping from the slope breccia at KO, however,
11 showed a 3.7°C variability (Spötl et al., 2002) which can be explained by the seasonal influence of the outside
12 air.

13 As we assume that the fractures were not influenced by seasonal changes in air temperature, the $\delta^{18}\text{O}$ signal of
14 the Vinschgau flowstones is primarily regarded as a proxy for $\delta^{18}\text{O}$ of local precipitation. This signal, however,
15 may be modified to a variable extent by in-aquifer processes discussed in 5.2.

16 5.1.2 $\delta^{13}\text{C}$

17 The interpretation of the carbon isotope signal of speleothems from karst caves is commonly more challenging
18 than that of $\delta^{18}\text{O}$ (e.g. McDermott, 2004), since $\delta^{13}\text{C}$ values can be affected by a variety of processes including
19 carbon dynamics of the soil and epikarst, subsurface air ventilation, and associated kinetic isotope fractionation.
20 Today, the Sonnenberg slope is mainly covered by sandy pararendzinas (Florineth, 1974) and contains a semi-
21 arid vegetation. The strong soil moisture deficit on the slopes (Della Chiesa et al., 2014) may limit the amount of
22 solutes entering the fracture system (Fairchild and Baker, 2012). Additionally, some of the carbonate is derived
23 from the crystalline host rock, in particular local occurrences of Fe-carbonates (Spötl et al., 2002).

24 Although carbon isotopes mostly follow the fluctuations of $\delta^{18}\text{O}$, this relationship can vary within a given
25 sample (e.g. LAS 19). LAS 19 shows a $\delta^{18}\text{O}$ rise of 3.2 ‰ at the YD-Holocene transition, followed by a similar
26 decrease in carbon isotopes, suggesting that during certain time intervals carbon isotopes may reflect a soil
27 signal, whereby more enriched $\delta^{13}\text{C}$ values correspond to an increase in soil bioproductivity (Genty et al., 2001;
28 Fairchild and Baker 2012; Borsato et al, 2015). As discussed below this signal is, however, masked by in-aquifer
29 processes as indicated by the co-variation of $\delta^{18}\text{O}$ and $\delta^{13}\text{C}$ isotopes.

30 5.2 Aquifer-internal processes

31 In a subsurface fracture system like the Sonnenberg where speleothems form as vein-filling calcite and
32 aragonite, prior calcite precipitation (PCP) and/or prior aragonite precipitation (PAP) are expected to influence
33 the stable isotope composition of speleothems. Both processes would result in the progressive joint enrichment
34 of ^{13}C and ^{18}O (Dreybrodt and Scholz, 2011; Fairchild and Baker, 2012).

35 Evaporation-induced kinetic fractionation is also likely to have an effect on the stable isotope values of calcite
36 and aragonite flowstones since evaporation and associated CO_2 degassing are the primary drivers of secondary
37 carbonate deposition. Nevertheless, stable isotope and temperature monitoring of a shallow underground pool
38 and its associated actively forming calcite speleothem indicates that calcite precipitation occurs close to isotopic
39 equilibrium with respect to $\delta^{18}\text{O}$, while $\delta^{13}\text{C}$ levels strongly deviate from equilibrium (Spötl et al., 2002). This is



1 also supported by the fact that even though carbon and oxygen isotopes show a covariance in several flowstones,
2 calcite samples and LAS 1 do not exhibit co-varying $\delta^{13}\text{C}$ and $\delta^{18}\text{O}$ values. Similarities in the absolute $\delta^{18}\text{O}$
3 values of the three TR samples (LAS 1, LAS 2 and LAS 21) further corroborate this, suggesting that even though
4 PCP/PAP occurred along the flow path, flowstone precipitation occurred close to isotopic equilibrium.
5 Therefore, we propose that kinetic fractionation likely had a negligible influence on the $\delta^{18}\text{O}$ of speleothem
6 calcite. In contrast, given that $\delta^{13}\text{C}$ and $\delta^{18}\text{O}$ values co-vary in the aragonite samples (LAS 34 and LAS 72) and
7 also in LAS 2 independent of its mineralogy (Fig. 3), it is likely that these samples formed out of isotopic
8 equilibrium.

9 To analyse the potential influence of kinetic processes and local hydrology on the isotopic composition of the
10 Vinschgau flowstones, coeval sections were compared. Unfortunately, in all cases the common time window of
11 deposition is too short to provide reliable analyses using statistical methods (e.g. Fohlmeister, 2012).
12 Nevertheless, as the deposition of the three TR samples partly overlaps, intra-fracture variability can be tested on
13 decadal to centennial scales despite differences in growth rate and hence proxy data resolution. Given the
14 similarities in the range of $\delta^{18}\text{O}$ variability (Fig. 4), mineralogy, and the lack of fluorescent lamination, we
15 suggest that flowstones in a given fracture form under very similar conditions and therefore most probably
16 record the local climate signal. Differences in the absolute values of $\delta^{18}\text{O}$ and $\delta^{13}\text{C}$ are attributed to PAP and
17 PCP.

18 A stronger influence of the local hydrology and hence a lower climate signal/noise ratio is expected when
19 comparing flowstones from different sites (Fig. 5). Due to the inter-fracture variance in PCP/PAP calcite was
20 deposited at KO (sample LAS 19), while at the same time aragonite formed at the SQ site (sample LAS 72).
21 Still, their $\delta^{18}\text{O}$ pattern shares some similarities within the combined errors of the two age models, while $\delta^{13}\text{C}$ in
22 the aragonite specimen shows a much larger amplitude (8.9‰) than in the coeval calcitic one (3.6‰). This most
23 likely reflects the combined influence of kinetic isotopic fractionation and the difference in the fractionation
24 factor between the two polymorphs (Morse and Mackenzie, 1990; Frisia et al., 2002). Frisia et al. (2002)
25 reported that carbon isotopes are 2 to 3.4 ‰ higher in aragonite than in calcite at Grotte de Clamouse (S France).
26 $\delta^{13}\text{C}$ values similar to that of LAS 72 were reported from modern aragonite from Obstanser Eishöhle (2.4 to 7.0
27 ‰), an alpine cave in southern Austria (Spötl et al., 2016). Moreover, PCP (PAP) may have further increased the
28 $\delta^{13}\text{C}$ values in the Vinschgau sites.

29 **5.3 Potential as a palaeoclimate archive**

30 Similar to speleothems from karst caves in semiarid settings (e.g. Avigour et al., 1992; McMillan et al., 2005;
31 Hoffmann et al., 2016), fracture-filling flowstone from non-carbonate, climate-sensitive settings may provide a
32 useful record of palaeoaridity and palaeohydrology. Annually laminated flowstones (e.g. LAS 6) that formed in a
33 few meters depth may provide insights into changes in seasonality (Koltai et al., 2017), while those from deeper
34 fractures likely record changes on multi-decadal to centennial resolution and thus provide short snapshots of
35 local climate. This case study shows, however, that fracture-filling speleothems also record the inherent
36 heterogeneity of such fractured aquifers which may mask short-term climate signals.

37 The most widely used proxies of classical karst speleothems include stable oxygen and carbon isotopes, trace
38 elements, growth rate, and fabric changes (e.g. Frisia et al., 2003; McDermott, 2004; McMillan et al., 2005;
39 Wassenburg et al., 2012). Although the majority of speleothem-based climate reconstructions utilize calcite
40 speleothems, recent studies indicate that aragonites can also provide valuable proxies for past climate, including



1 seasonality (e.g. McMillan et al., 2005) and palaeorainfall variability (e.g. Wassenburg et al., 2012; Ridley et al.,
2 2015; Wassenburg et al., 2016). However, as aragonite is metastable at Earth's surface conditions and hence
3 susceptible to diagenetic transformation, the possible alteration of the geochemical signal has to be considered
4 (e.g. Domínguez-Villar et al., 2016 and references therein). Moreover, Lachniet (2015) emphasised that the $\delta^{18}\text{O}$
5 variability of aragonite speleothems should only be used as a proxy if aragonite precipitation occurred close to
6 isotopic equilibrium.

7 Thin section and XRD analyses indicate pristine aragonite in LAS 1, 2, 34 and 72. Aragonite preservation in
8 these samples is further supported by the fact that all ^{230}Th ages are in stratigraphic order regardless of
9 mineralogy (Suppl. Table 1). Nevertheless, flowstone deposition was most probably influenced by kinetic
10 isotope fractionation as suggested by the high correlation between carbon and oxygen isotopes in LAS 2, 34 and
11 72 (Fig. 3). Therefore, $\delta^{18}\text{O}$ variability should be interpreted carefully in these three samples.

12 Moreover, changes in speleothem mineralogy and growth rate are first and foremost driven by in-aquifer
13 processes including PCP and/or PAP, as indicated by the TR samples and LAS 19 and LAS 72 (Figs. 6 and 8).
14 Therefore, calcite-aragonite transitions and growth rate changes do not necessarily reflect an external (climate)
15 signal, unless coeval samples show a coherent pattern.

16 Carbon isotope data suggest a weak soil-derived signal for short time periods only (e.g. at the YD-to-Holocene
17 transition in LAS 19), while most values suggest buffering by inorganic carbon in conjunction with kinetic
18 isotope enrichment (Spötl et al., 2002).

19 The most prominent feature of $\delta^{18}\text{O}$ proxy record is the $\sim 3.2\%$ rise in LAS 19 at the YD-Holocene transition
20 (Fig. 6). Moreover, the first order pattern of the two aragonite samples covering the Bølling-Allerød warm phase
21 shows a close resemblance to the $\delta^{18}\text{O}$ variability of Greenland ice cores (Rasmussen et al., 2006) and to the
22 ostracod record from Mondsee (Lauterbach et al., 2011), a lake in central Austria, suggesting that centennial- to
23 orbital-scale large-amplitude changes of the Northern Hemisphere climate system are recorded in the $\delta^{18}\text{O}$
24 variability of this archive.

25 During the YD a gradual $\sim 1.7\%$ decline in $\delta^{18}\text{O}$ is observed in LAS 21 between 12.2 and 11.7 ka BP. Parts of
26 this shift are also captured by LAS 1 and LAS 19, implying a related cause. Several terrestrial archives across
27 Europe record a change in regional climate mid-way through the YD (e.g. Brauer et al., 2008; Bakke et al., 2009;
28 Baldini et al., 2015; Belli et al., 2016). The onset of this transition was time-transgressive (~ 12.45 to 12.15 ka
29 BP) across Europe due to the gradual northward shift of the polar front driven by the resumption of the North
30 Atlantic overturning (Lane et al., 2013; Bartolomé et al., 2015). Whether this shift towards more negative values
31 in our $\delta^{18}\text{O}$ record corresponds to the change in the regional climate or to in-aquifer processes remains unclear
32 given the lack of a flowstone sample covering the entire YD.

33 6 Conclusions

34 Petrographic and geochemical analyses of vein-filling calcite and aragonite flowstones in near-surface fractures
35 indicate that the latter polymorph is more susceptible to kinetic processes regarding both $\delta^{18}\text{O}$ and $\delta^{13}\text{C}$. The two
36 most important in-aquifer processes modifying the geochemical signature of these speleothems are evaporation
37 and PCP/PAP. Both of these processes are likely to govern variations in speleothem mineralogy, as indicated by
38 the deposition of coeval aragonite and calcite flowstones.



1 $\delta^{18}\text{O}$ variability has proved to be the most reliable climate proxy in the Vinschgau flowstones. Low-amplitude,
2 high-frequency (decadal-scale) variability in LAS 1, 6, 10, 19 and 21 is attributed to in-aquifer processes, while
3 the centennial-scale variability shows significant variation (e.g. 3.2‰) suggesting changing hydrological
4 conditions. Although local factors, such as strong evaporation and PCP/PAP can amplify these climate
5 signatures, the $\delta^{18}\text{O}$ values show a broadly similar pattern to regional $\delta^{18}\text{O}$ lacustrine records (e.g. Mondsee).
6 Due to the lack of long overlapping sections of speleothem growth and the complexity of in-aquifer processes
7 this case study shows that it is highly challenging to establish a robust stacked $\delta^{18}\text{O}$ record of local climate
8 change on multi-millennial to orbital timescales using such speleothems. However, it is possible that fracture-
9 filling calcite and/or aragonite from other areas may have a high potential as a climate archive if the local
10 hydrogeological conditions are well constrained. Our study also emphasises that a tight age control and a multi-
11 proxy approach are essential in the study of such non-karstic settings.

12 **Acknowledgements**

13 This project was supported by the Autonome Provinz Bozen-Südtirol (no. 16/40.3). D. Schmidmair is
14 acknowledged for XRD analyses and K. Wendt for linguistic help and valuable comments.

15 **References**

- 16
17 Alley, R.B., Meese, D.A., Shuman, C.A., Gow, A.J., Taylor, K.C., Grootes, P.M., White, J.W.C., Ram, M.,
18 Waddington, E.D., Mayewski, P.A. and Zielinski, G.A.: Abrupt increase in Greenland snow accumulation at the
19 end of the Younger Dryas event. *Nature*, 362, 527–529, 1993.
- 20 Avigour, A., Magaritz, M. and Issar, A.: Pleistocene paleoclimate of the arid region of Israel as recorded in
21 calcite deposits along regional transverse faults and in veins. *Quaternary Res.*, 37, 304–314, 1992.
- 22 Bakke, J., Lie, O., Heegaard, E., Dokken, T., Haug, G.H., Birks, H.H., Dulski, P. and Nilsen, T.: Rapid oceanic
23 and atmospheric changes during the Younger Dryas cold period. *Nature Geoscience*, 2, 202–205, 2009.
- 24 Boch, R., Cheng, H., Spötl, C., Edwards, R.L., Wang, X. and Häuselmann, P.: NALPS: a precisely dated
25 European climate record 120–60 ka. *Clim. Past*, 7, 1247–1259, 2011.
- 26 Brauer, A., Haug, G.H., Dulski, P., Sigman, D.M. and Negendank, J.F.W.: An abrupt wind shift in western
27 Europe at the onset of the Younger Dryas cold period. *Nature Geoscience*, 1, 520–523, 2008.
- 28 Broecker, W.S., Denton, G.H., Edwards L.R., Cheng, H., Alley, R.B. and Putnam, A.E.: Putting the Younger
29 Dryas cold event into context. *Quaternary Sci. Rev.*, 29, 1078–1081, 2010.
- 30 Cheng, H., Edwards, R.L., Shen, C.-C., Polyak V.J., Asmerom, Y., Woodhead, J., Hellstrom, J., Wang, Y., Kong,
31 X., Spötl, C., Wang, X. and Calvin Alexander, Jr. E.: Improvements in ^{230}Th dating, ^{230}Th and ^{234}U half-life
32 values, and U-Th isotopic measurements by multi-collector inductively coupled plasma mass spectrometry.
33 *Earth Planet. Sc. Lett.*, 371–372, 82–91, 2013.
- 34 Cheng, H., Edwards, R.L., Sinha, A., Spötl, C., Yi, L., Chen, S., Kelly, M., Kathayat, G., Wang, X., Li, X.,
35 Kong, X., Wang, Y., Ning, Y. and Zhang, H.: The Asian monsoon over the past 640,000 years and ice age
36 terminations. *Nature*, 534, 640–646, 2016.
- 37 Dansgaard, W., White, J.W.C. and Johnsen, S.J.: The abrupt termination of the Younger Dryas event. *Nature*,
38 339, 532–533, 1989.



- 1 Della Chiesa, S., Bertoldi, G., Niedrist, G., Obojes, N., Endrizzi, S., Albertson, J.D., Wohlfahrt, G., Hörtnagl, L.
2 and Tappeiner, U.: Modelling changes in grassland hydrological cycling along an elevational gradient in the
3 Alps. *Ecohydrology*, 7, 1453-1473, 2014.
- 4 Dreybrodt, W. and Scholz, D.: Climatic dependence of stable carbon and oxygen isotope signals recorded in
5 speleothems: From soil water to speleothem calcite. *Geochim. Cosmochim. Ac.*, 75, 734-752, 2011.
- 6 Domínguez-Villar, D., Krklec, K., Pelicon, P., Fairchild, I.J., Cheng, H. and Edwards, L.R.: Geochemistry of
7 speleothems affected by aragonite to calcite recrystallization – Potential inheritance from the precursor mineral.
8 *Geochim. Cosmochim. Ac.*, 200, 310-329, 2017.
- 9 Edwards, R. L., Chen, J. H. and Wasserburg, G. J.: ^{238}U , ^{234}U , ^{230}Th , ^{232}Th systematics and the precise
10 measurement of time over the past 500,000 years. *Earth Planet. Sc. Lett.*, 81, 171-192, 1987.
- 11 Fairchild, I.J. and Baker, A.: *Speleothem science: from processes to past environments*. Wiley-Blackwell,
12 Oxford, 2012.
- 13 Fliri, F.: *Das Klima der Alpen im Raume von Tirol*: Innsbruck, Universitäts-Verlag Wagner, 1975.
- 14 Florineth, F.: *Vegetation und Boden im Steppengebiet des oberen Vinschgaues (Südtirol, Italien)*:
15 *Naturwissenschaftlich-medizinischer Verein Innsbruck Berichte*, 61, 43–70, 1974.
- 16 Fohlmeister, J., Schröder-Ritzrau, A., Scholz, D., Spötl, C., Riechelmann, D. F. C., Mudelsee, M., Wackerbarth,
17 A., Gerdes, A., Riechelmann, S., Immenhauser, A., Richter, D. K. and Mangini, A.: Bunker Cave stalagmites: an
18 archive for central European Holocene climate variability. *Clim. Past*, 8, 1751–1764, 2012.
- 19 Frisia, S., Borsato, A., Fairchild, I.J., McDermott, F. and Selmo, E.M.: Aragonite-calcite relationships in
20 speleothems (Grotte de Clamouse, France): environment, fabrics, and carbonate geochemistry. *J. Sed. Res.*, 72,
21 687-699, 2002.
- 22 Frisia, S., Borsato, A., Preto, N. and McDermott, F.: Late Holocene annual growth in three Alpine stalagmites
23 records the influence of solar activity and the North Atlantic Oscillation on winter climate. *Earth Planet. Sc.*
24 *Lett.*, 216, 411-424, 2003.
- 25 Frisia, S.: Microstratigraphic logging of calcite fabrics in speleothems as tool for palaeoclimate studies. *Int. J.*
26 *Speleol.* 44, 1-16, 2015.
- 27 Frisia, S., Weirich, L., Hellstrom, J., Borsato, A., Gолledge, N.R., Anesio, A.M., Bajo, P., Drysdale, R.N.,
28 Augustinus, P.C., Rivard, C. and Cooper, A.: The influence of Antarctic subglacial volcanism on the global iron
29 cycle during the Last Glacial Maximum. *Nature Communications*, 8:15425, DOI: 10.1038/ncomms15425, 2017.
- 30 Ford, D.C. and Williams, P.W.: *Karst Geomorphology and Hydrology*. Unwin Hyman, London, 1989.
- 31 Genty, D., Baker, A., Massault, M., Proctor, C., Gilmour, M., Pons-Branchu, E. and Hamelin, B.: Dead carbon
32 in stalagmites: carbonate bedrock paleodissolution vs. aging of soil organic matter. Implications for ^{13}C
33 variations in speleothems. *Geochim. Cosmochim. Ac.*, 65, 3443–3457, 2001.
- 34 Heiri, O., Koinig, K.A., Spötl, C., Barrett, S., Brauer, A., Drescher-Schneider, R., Gaar, D., Ivy-Ochs, S.,
35 Kerschner, H., Luetscher, M., Moran, A., Nicolussi, K., Preusser, F., Schmidt, R., Schoeneich, P., Schwörer, C.,
36 Sprafke, T., Terhorst, B. and Tinner, W.: Palaeoclimate records 60–8 ka in the Austrian and Swiss Alps and their
37 forelands. *Quaternary Sci. Rev.* 106, 186-205, 2014.
- 38 Hoffmann, D.L., Rogerson, M., Spötl, C., Luetscher, M., Vance, D., Osborne, A., Fello, N. and Moseley, G.:
39 Timing and causes of North African wet phases during the last glacial period and implications for modern human
40 migration. *Scientific Reports* 6: 36367, doi: 10.1038/srep36367, 2016.



- 1 Ilyashuk, B., Gobet, E., Heiri, O., Lotter, A.F., van Lewuwen, J. F.N., van der Knaap, W.O., Ilyashuk, E.,
2 Oberili, F. and Ammann, B.: Lateglacial environmental and climatic changes at the Maloja Pass, Central Swiss
3 Alps, as recorded by chironomids and pollen. *Quaternary Sci. Rev.*, 28, 1340-1353, 2009.
- 4 Johnson, K.R., Hu, C., Belshaw, N.S. and Henderson, G.M.: Seasonal trace-element and stable isotope variations
5 in a Chinese speleothem: the potential for high resolution paleomonsoon reconstruction. *Earth Planet. Sci. Lett.*,
6 244, 394-407, 2006.
- 7 Kelly, S.D., Newville, M.G., Cheng, L., Kemner, K.M., Sutton, S.R., Fenter, P., Sturchio, N.C. and Spötl, C.:
8 Uranyl incorporation in natural calcite. *Environmental Science & Technology*, 37, 1284-1287, 2003.
- 9 Kendall, A.C.: Radial fibrous calcite: a reappraisal. In: Schneidermann, N., Harris, P.M. (Eds.), *Carbonate*
10 *Cements*. SEPM Special Publication 36, pp. 59-77, 1985.
- 11 Kerschner, H., Kaser, G. and Sailer, R.: Alpine Younger Dryas glaciers as palaeo-precipitation gauges. *Ann.*
12 *Glaciol.*, 31, 80-84, 2000.
- 13 Kerschner, H. and Ivy-Ochs, S.: Palaeoclimate from glaciers: Examples from the Eastern Alps during the Alpine
14 Lateglacial and early Holocene. *Global and Planetary Change*, 60, 58–71, 2008.
- 15 Koltai, G., Spötl, C., Luetscher, M., Barrett S.J. and Müller, W.: The nature of annual lamination in carbonate
16 flowstones from non-karstic fractures, Vinschgau (northern Italy). *Chem. Geol.*, 457, 1-14, 2017.
- 17 Lachniet, M.S., Bernal, J.P., Asmerom, Y. and Polyak, V.: Uranium loss and aragonite-calcite age discordance in
18 a calcitized aragonite stalagmite. *Quaternary Geochronol.*, 14, 26-37, 2012.
- 19 Lachniet, M.S.: Are aragonite stalagmites reliable palaeoclimate proxies? Test for oxygen isotope time-series
20 replication and equilibrium. *Geol. Soc. Am. Bull.*, 127, 1521-1533, 2015.
- 21 Lane, C.S., Brauer, A., Blockley, S.P.E. and Dulski, P.: Volcanic ash reveals time-transgressive abrupt climate
22 change during the Younger Dryas. *Geology*, 41, 1251–1254, 2013.
- 23 Lauterbach, S., Brauer, A., Andersen, N., Danielopol, D.L., Dulski, P., Hüls, M., Milecka, K., Namiotko, T.,
24 Obremska, M., von Grafenstein, U. and Declakes participants: Environmental responses to Lateglacial climatic
25 fluctuations recorded in the sediments of pre-Alpine Lake Mondsee (northeastern Alps). *J. Quaternary Sci.*, 26,
26 253-267, 2011.
- 27 Luetscher, M., Boch, R., Sodemann, H., Spötl, C., Cheng, H., Edwards, L.R., Frisia, S., Hof, F. and Müller, W.:
28 North Atlantic storm track changes during the Last Glacial Maximum recorded by Alpine speleothems. *Nature*
29 *Communication*, 6: 6344, doi: 10.1038/ncomms7344, 2015.
- 30 McDermott, F.: Palaeo-climate reconstruction from stable isotope variations in speleothems: a review.
31 *Quaternary Sci. Rev.*, 23, 901-918, 2004.
- 32 McMillan, E.A., Fairchild, I.J., Frisia, S., Borsato, A. and McDermott, F.: Annual trace element cycles in
33 calcite–aragonite speleothems: evidence of drought in the western Mediterranean 1200–1100 yr BP. *J.*
34 *Quaternary Sci.*, 20, 423-433, 2005.
- 35 Morse, J.W. and Mackenzie, F.T.: *Geochemistry of sedimentary carbonates*. *Developments in Sedimentology*,
36 48, Elsevier, Amsterdam, 1990.
- 37 Ostermann, M., Koltai, G., Cheng, H. and Spötl, C.: Speleothems constrain the onset of deep-seated gravitational
38 slope deformations, Vinschgau (Italian Alps). *Landslides* (submitted).
- 39 Rasmussen, S.O., Andersen, K.K., Svensson, A.M., Steffensen, J.P., Vinther, B.M., Clausen, H.B., Siggaard-
40 Andersen, M.-L., Johnsen, S.J., Larsen, L.B., Dahl-Jensen, D., Bigler, M., Röthlisberger, R., Fischer, H., Goto-



- 1 Azuma, K., Hansson, M.E. and Ruth, U.: A new Greenland ice core chronology for the last glacial termination,
2 *J. Geophys. Res.*, 11, D06102, doi:10.1029/2005JD006079, 2006.
- 3 Richards, D. and Dorale, J.A.: Uranium-series chronology and environmental applications of speleothems. In:
4 Bourdon, B., Henderson, G., Lundstorm, C.C. and Turner, S. (Eds.), *Uranium-series geochemistry, Reviews in*
5 *Mineralogy and Geochemistry*, 52, 407-460, Washington, D.C. (Min. Soc. Amer.), 2003.
- 6 Richter, D., Neuser, R.D., Schreuer, J., Gies, A. and Immenhauser, A.: Radial fibrous calcites: A new look at
7 an old problem. *Sediment. Geol.*, 239, 23-36, 2011.
- 8 Ridley, H.E., Asmerom, Y., Baldini, J.U.L., Breitenbach, S.F.M., Aquino, V.V., Pruffer, K.M., Culleton, B.J.,
9 Polyak, V., Lechleitner, F.A., Kennett, D.J., Zhang, M., Marwan, N., Macpherson, C.G., Baldini, L.M., Xiao, T.,
10 Peterkin, J.L., Awe, J. and Haug, G.H.: Aerosol forcing of the position of the intertropical convergence zone
11 since AD1550. *Nature Geoscience*, 8, 195-200, doi:10.1038/ngeo2353, 2015.
- 12 Scholaut, G., Brauer, A., Nakagawa, T., Lamb, H. F., Tyler, J.J., Staff R.A., Marshall, M.H., Ramsey, C.B.,
13 Bryant, C.L. and Tarasov, P.E.: Evidence for a bi-partition of the Younger Dryas Stadial in East Asia associated
14 with inversed climate characteristics compared to Europe. *Scientific Reports* 7: 44983, doi:10.1038/srep44983,
15 2017.
- 16 Scholz, D. and Hoffmann, D.: ²³⁰Th/U-dating of fossil corals and speleothems. *Quaternary Science Journal* 57,
17 52-76, 2008.
- 18 Scholz, D. and Hoffman, D.: StalAge – An algorithm designed for construction of speleothem age models.
19 *Quaternary Geochronology* 6, 369-382, 2011.
- 20 Shen, C.C., Wu, C.C., Cheng, H., Edwards, R.L., Hsieh, Y-T., Gallet, S., Chang, C.C., Li, T.Y., Lam, D.D.,
21 Kano, A., Hori, M. and Spötl, C.: High-precision and high resolution carbonate ²³⁰Th dating by MC-ICP-MS
22 with SEM protocols. *Geochim. Cosmochim. Ac.* 99, 71-86, 2012.
- 23 Spötl, C., Unterwurzacher, M., Mangini, A. and Longstaffe, F.J.: Carbonate speleothems in the dry, inneralpine
24 Vinschgau valley, northernmost Italy: Witnesses of changes in climate and hydrology since the Last Glacial
25 Maximum. *J. Sediment. Res.*, 72, 793-808, 2002.
- 26 Spötl, C.: Long-term performance of the Gasbench isotope ratio mass spectrometry system for the stable isotope
27 analysis of carbonate microsamples. *Rapid Commun. Mass Spectrom.*, 25, 1683-1685, 2011.
- 28 Spötl, C., Fohlmeister, J., Cheng, H. and Boch, R.: Modern aragonite formation at near-freezing conditions in an
29 alpine cave, Carnic Alps, Austria. *Chem. Geol.*, 435, 60-70, 2016.
- 30 von Grafenstein, U., Erlenkeuser, H., Brauer, A., Jouzel, J. and Johnsen, S.J.: A mid-European decadal isotope-
31 climate record from 15,500 to 5000 years B.P. *Science* 284, 1654–1657, 1999.
- 32 von Grafenstein, U., Belmecheri, S., Eicher, U., van Raden, U.J., Erlenkeuser, H., Andersen, N. and Ammann
33 B.: The oxygen and carbon isotopic signatures of biogenic carbonates in Gerzensee, Switzerland, during the
34 rapid warming around 14,685 years BP and the following interstadial. *Palaeogeogr., Palaeoclimatol.,*
35 *Palaeoecol.*, 391, 25-32, 2013.
- 36 ZAMG: *Das Klima von Tirol-Südtirol-Belluno, Vienna (Zentralanstalt für Meteorologie und Geodynamik)*,
37 2015.
- 38 Wang, P.X., Wang, B., Cheng, H., Fasullo, J., Guo, Z.T., 6, Kiefer, T. and Liu, Z.Y.: The global monsoon across
39 timescales: coherent variability of regional monsoons. *Clim. Past*, 10, 2007-2052, 2014.



- 1 Wassenburg, J.A., Immenhauser, A., Richter, D.K., Jochum, K.P., Fietzke, J., Deininger, M., Goos, M., Scholz,
- 2 D. and Sabaoui, A.: Climate and cave control on Pleistocene/Holocene calcite-to-aragonite transitions in
- 3 speleothems in Morocco: Elemental and isotopic evidence. *Geochim. Cosmochim. Ac.*, 92, 23-47, 2012.
- 4 Wassenburg, J.A., Scholz, D., Jochum, K.P., Cheng, H., Oster, J., Immenhauser, A., Richter, D.K., Häger, T.,
- 5 Jamieson, R.A., Baldini, J.U.L., Hoffmann, D. and Breitenbach, S.F.M.: Determination of aragonite trace
- 6 element distribution coefficients from speleothem calcite-aragonite transitions. *Geochim. Cosmochim. Ac.*, 190,
- 7 347-367, 2016.
- 8 Webb, M., Dredge, J., Barker, P.A., Müller, W., Jex, C., Desmarchelier, J., Hellstrom, J. and Wynn, P.M.:
- 9 Quaternary climatic instability in south-east Australia from a multi-proxy speleothem record. *J. Quaternary Sci.*,
- 10 29, 589-596, 2014.
- 11 Wedepohl, K.H.: The composition of the continental crust. *Geochim. Cosmochim. Ac.*, 59, 1217-1239, 1995.
- 12 Wurth, G., Niggemann, S., Richter D. K. and Mangini A.: The Younger Dryas and Holocene climate record of a
- 13 stalagmite from Hölloch Cave (Bavarian Alps, Germany). *J. Quaternary Sci.*, 19, 291-298, 2004.



Table 1. Stable isotope composition of the Vinschgau flowstones.

Sample	$\delta^{18}\text{O}$ (‰)			$\delta^{13}\text{C}$ (‰)		
	min.	max.	Mean	min.	max.	Mean
<i>TR</i>						
LAS 1	-12.8	-11.1	-11.9	-2.2	4.3	-0.2
LAS 2	-13.0	-9.7	-11.7	-2.3	7.3	0.9
LAS 21	-13.1	-9.8	-12.1	-2.3	2.4	-0.7
<i>SQ</i>						
LAS 6	-14.1	-11.8	-13.2	-2.9	-0.3	-2.1
LAS 34	-12.8	-9.9	-11.3	-1.0	6.2	2.2
LAS 72	-11.8	-9.2	-10.7	-1.8	7.3	1.6
<i>KO</i>						
LAS 10	-12.3	-10.3	-11.3	-5.6	-1.4	-3.2
LAS 19	-13.5	-10.1	-11.7	-4.5	-0.8	-2.8

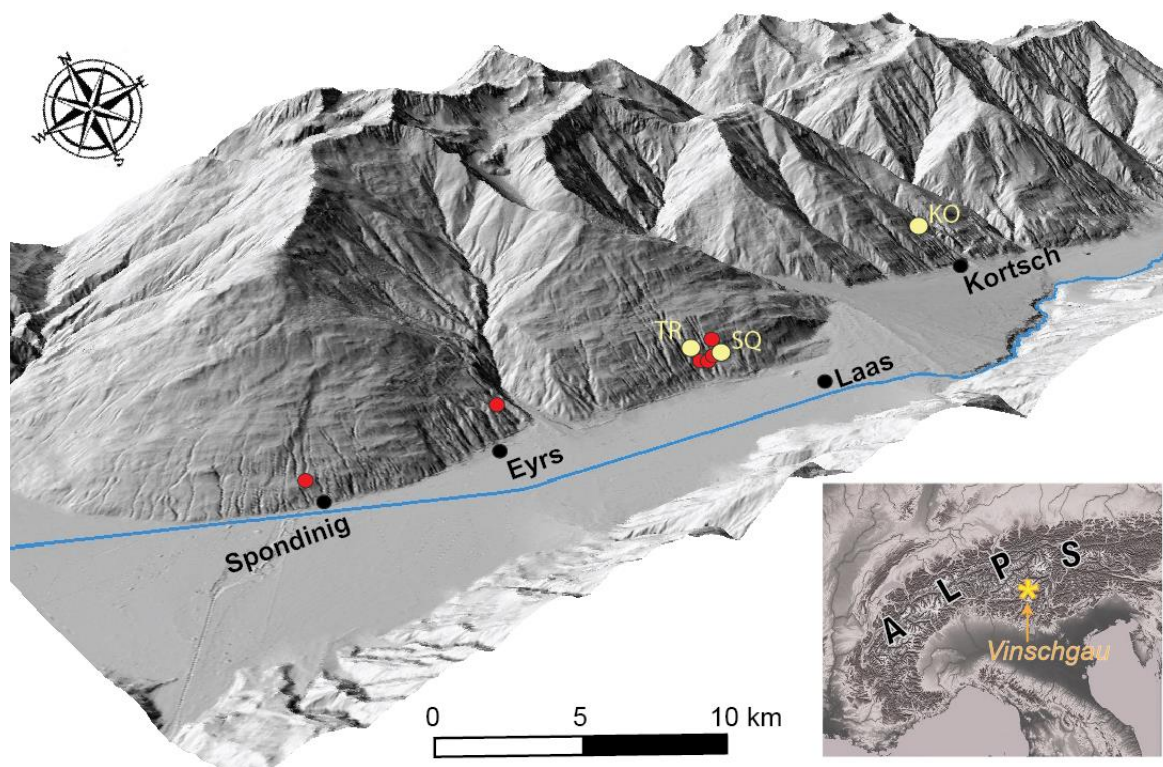
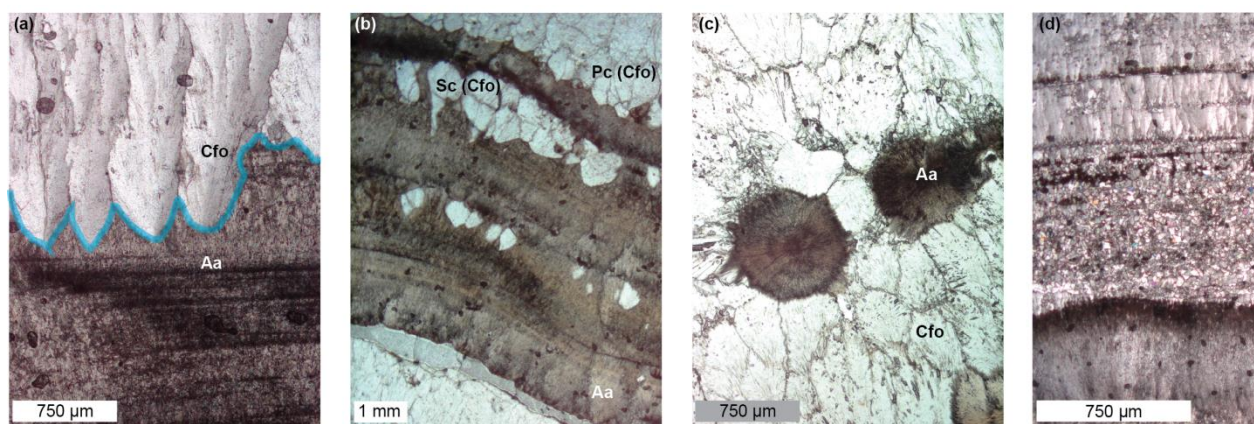


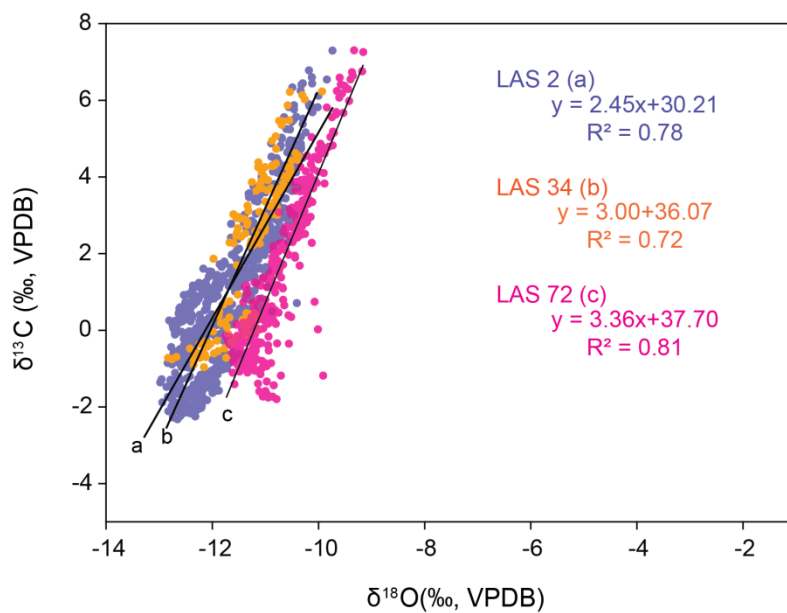
Figure 1: Oblique view of the Vinschgau valley. Red points show the occurrence of vein-filling flowstones in the lower part of the south-facing slope (Sonnenberg). Yellow points mark the three sampling sites.



5 Figure 2: Aragonite and calcite textures. (a) Boundary of fascicular optic calcite (Cfo) and acicular aragonite (Aa), showing competing crystal growth between the two polymorphs (blue line, sample LAS 2). (b) Fascicular optic calcite of primary (Pc(Cfo)) and secondary origin (Sc(Cfo), sample LAS 2). (c) Co-precipitation of primary calcite and aragonite (sample LAS 21). (d) Complex fabric dominated by mosaic calcite (Cm) where fascicular optic calcite



polycrystals (Cfo) are locally present between acicular aragonite (Aa) and fascicular optic calcite (Cfo, sample LAS 34).



5 **Figure 3: Isotopic crossplot for LAS 2, LAS 34 and LAS 72. The highly significant correlation between the two isotopes suggests strong kinetically controlled isotope fractionation.**

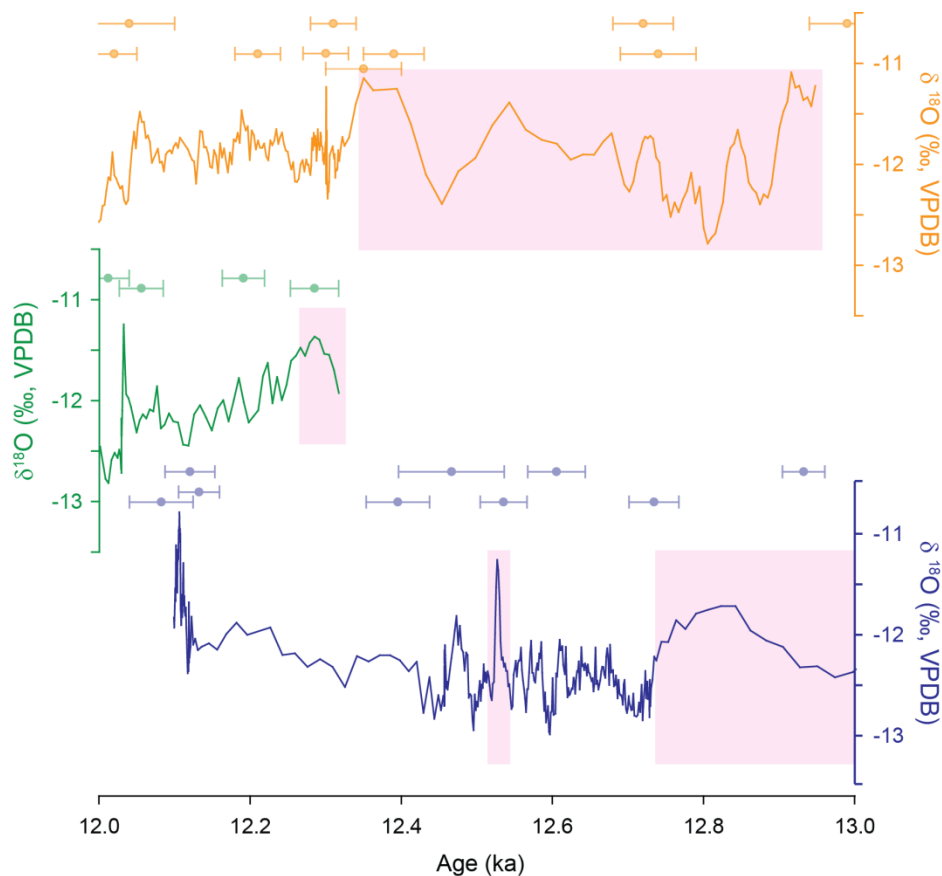


Figure 4: $\delta^{18}\text{O}$ variability of the TR samples LAS 1 (orange), LAS 21 (green) and LAS 2 (blue) in their overlapping sections. All samples are plotted based on the modelled ages. ^{230}Th ages with their corresponding 2 errors are plotted above each $\delta^{18}\text{O}$ time series. Pink rectangles indicate aragonite fabric.

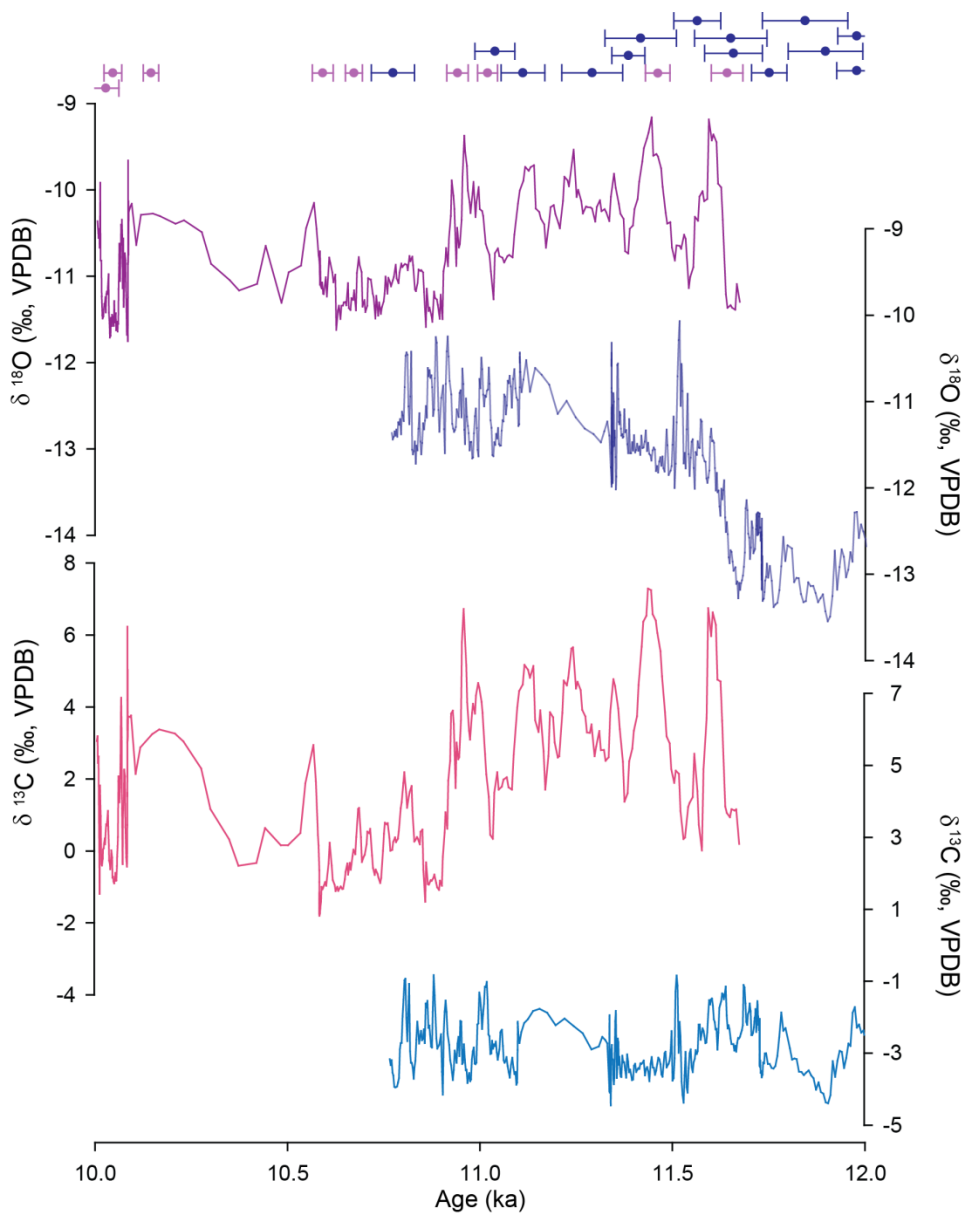
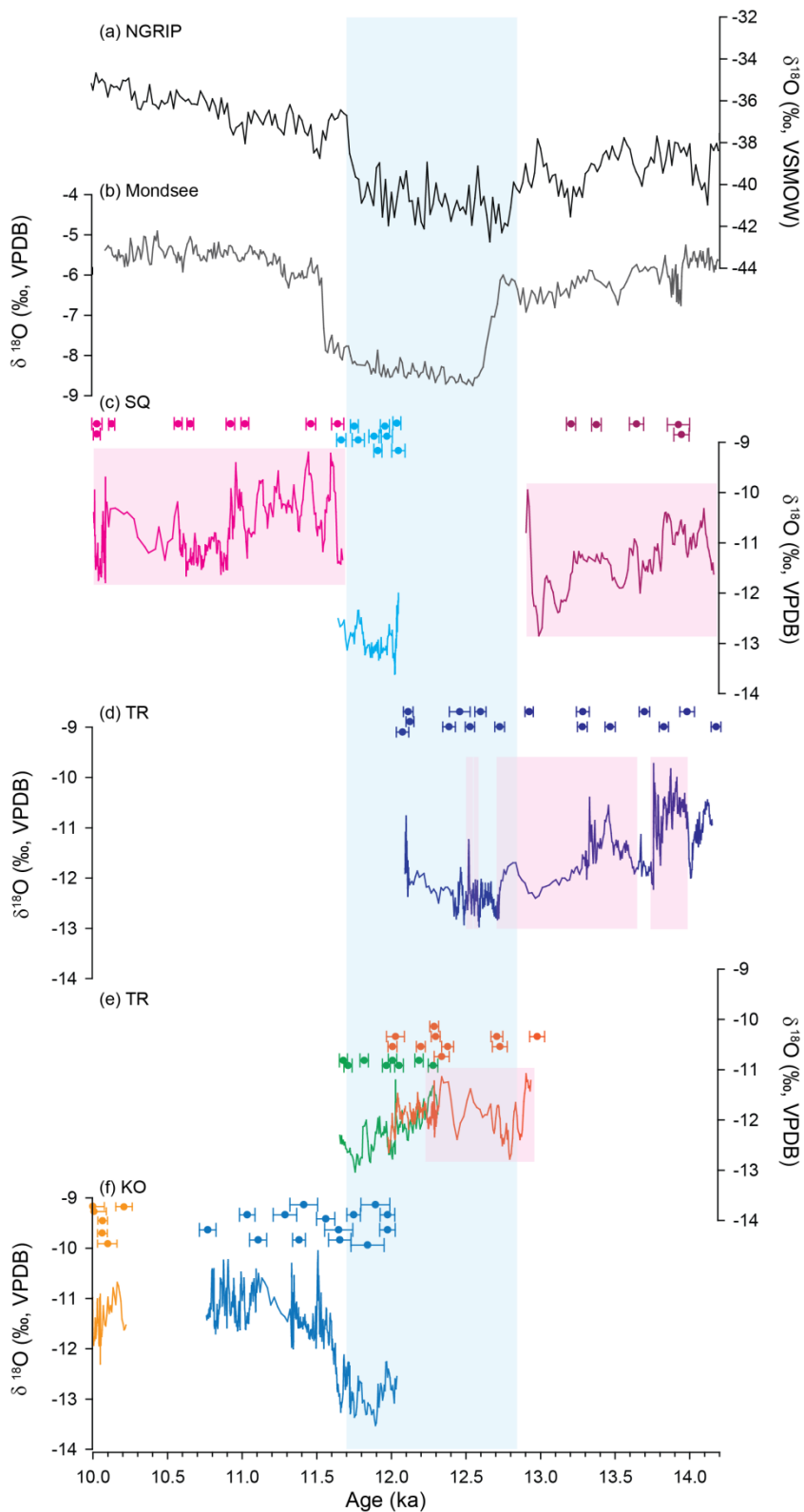


Figure 5: Stable isotope variability of LAS 72 (pink) and LAS 19 (blue) between 12 and 10 ka, BP. Note that LAS 72 is comprised of aragonite, while LAS 19 is a calcitic flowstone.





5 **Figure 6: Comparison of $\delta^{18}\text{O}$ time-series of (a) the NGRIP ice core (Rasmussen et al., 2006), (b) benthic ostracods from Mondsee (Lauterbach et al., 2011) and the Vinschgau flowstones (c-f). (c) shows the three samples from SQ site: LAS 72 (bright pink), LAS 6 (turquoise) and LAS 34 (dark pink). The $\delta^{18}\text{O}$ variability of the TR samples is shown in (e) and (d), whereby dark blue represents the of LAS 2, green and orange mark the oxygen isotope record of LAS 21 and LAS 1, respectively. LAS 10 (yellow) and LAS 19 (light blue) from KO are shown in (f). Note that the pink rectangles are indicative of aragonite.**